# A practical device to determine the reflection coefficient of acoustic materials in-situ based on a Microflown and microphone sensor

**R. Lanoye**[1a]**, H.-E. de Bree**[b]**, W. Lauriks**[a] **and G. Vermeir**[a]
[1] Aspirant van het Fonds voor Wetenschappelijk Onderzoek - Vlaanderen
[a] Laboratory of acoustics and thermal physics, Katholieke Universiteit Leuven, Celestijnenlaan 200D, B-3001 Heverlee, Belgium
e-mail: **reinhilde.lanoye@bwk.kuleuven.ac.be**
[b] Microflown Technologies, PO BOX 300, 6900 AH Zevenaar, The Netherlands,
www.microflown.com, debree@microflown.com

## Abstract
The reflection coefficient of acoustic absorbing materials is often measured in a standing wave tube. This method has some drawbacks. Here a novel technique, that is capable to determine the reflection coefficient in a fast way in-situ, real time, oblique and without the use of a standing wave tube, is presented. The method is based on the simultaneous measurement of normal acoustical particle velocity and sound pressure at the same position. These values are determined with the use of a Microflown (Titan sensor-element) and a sound pressure microphone. Theory is presented and supported by verifying measurements.

## 1 Introduction

In order to obtain a good acoustical climate in buildings and rooms, lots of acoustic absorbing materials are used. To model the performance of these materials in practice, researchers are interested in the reflection coefficient for different angles of sound incidence. Most techniques used to determine the angle dependent reflection coefficient make use of a measurement of sound pressure at different positions and/or particle velocity, together with an assumption of the exact nature of the wave field at the measurement position(s). The accuracy of the calculated reflection coefficient depends on the measurement precision and the exactness of the assumption of the pressure field.
A proven technique to determine the angle dependency of the reflection coefficient is described by Tamura [1]. In this method, sound pressure is measured in two planes and a two dimensional Fourier transformation is used to calculate the angle dependent reflection coefficient. Thus, no assumptions about the exact nature of the wave field are made. However, a drawback of the method is the rather complicated measurement setup, the need for a large test sample and long measuring times. Nowadays, the alternative techniques are also based on the measurement of sound pressure [1, 2].
In this article, a new technique for determining the reflection coefficient, based on the simultaneous measurement of sound pressure and particle velocity, is described. In a first paragraph, a brief description of the measurement principle and calibration mechanism of the particle velocity is presented. A comparison of measurements in Kundt's tube with the new technique and with a known pp-technique, described by Chu [3], is given. Afterwards, results of measurements in a semi-anechoic room, executed with the new technique and with the Tamura technique are shown.

# 2 Microflown

The Microflown, developed by de Bree et al. [4, 5], is that part of the pu-probe which measures the acoustic particle velocity. The measurement principle of the device is based on the temperature difference between two resistive sensors. A travelling acoustic wave causes a heat transfer from one sensor to the other and the temperature difference at the sensors, induced by the acoustic wave, causes a differential electrical resistance variation which is measured.
Inherent in the physical working principle of the transducer, the frequency response of the Microflown decreases with frequency due to diffusion effects and heat capacity. The sensitivity of the Microflown can be approximated by formula (1).

$$S_{Microflown} = \frac{lfs}{\sqrt{1+\frac{f_e^2}{f^2}}\sqrt{1+\frac{f^2}{f_d^2}}\sqrt{1+\frac{f^2}{f_{hc}^2}}} \tag{1}$$

$lfs$ $[\frac{mV}{Pa} \cdot \rho_o c]$ is the sensitivity of the Microflown at $250\,Hz$. $f_d$ and $f_{hc}$ are roll-off frequencies caused by diffusion effects and thermal inertia. $f_e$ is a roll off at a low frequency. This roll off has a typical frequency in the range $30 - 100\,Hz$, $f_d$ lies typically in the range $700 - 1500\,Hz$, $f_{hc}$ has a higher value ($4000\,Hz$ to $\infty$).
In the pu-probe of Microflown Technologies, a Microflown sensor and a miniature pressure microphone are placed close together. With this pu-probe, impedance can be measured directly.
The phase difference of a Microflown relative to the included microphone can be approximated by formula (2).

$$Phase_{Microflown} = \arctan\frac{C_1}{f} - \arctan\frac{f}{C_2} - \arctan\frac{f}{C_3} \tag{2}$$

$C_1 \simeq f_e$, $C_2 \simeq f_d$ and $C_3 \simeq f_{hc}$.

## 2.1 Calibration

Several calibration methods can be used. The standing wave tube calibration is used for lower frequencies ($30\ Hz$ - $4\ kHz$). A calibration in a semi-anechoic room can be used in the frequency range $200\,Hz - 20\,kHz$.

### 2.1.1 Kundt's tube

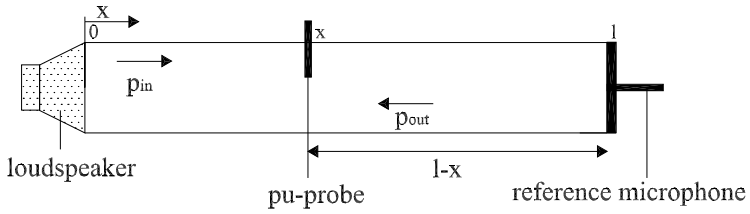


Figure 1: calibration of pu-probe in standing wave tube

In figure (1) a standing wave tube with a perfect reflecting ending is drawn. In this tube, the pressure at a position $x$ is given by $p(x,t,\omega) = (Ae^{-ikx} + Be^{ikx})e^{i\omega t}$. The particle velocity is given by $u(x,t,\omega) = \frac{-1}{i\omega\rho_o}\frac{\partial p(x,t,\omega)}{\partial x} = (\frac{Ae^{-ikx}}{\rho_o c} - \frac{Be^{ikx}}{\rho_o c})e^{i\omega t}$.
To calibrate the pu-probe, a reference microphone is placed at the rigid reflecting ending ($x = l : u(l) = 0$) of

the standing wave tube. At the other end, a loudspeaker is placed, so $p(0) = p_o$. These boundary conditions lead to formulae (3) and (4) for pressure and particle velocity at a position $x$ in the tube respectively.

$$p(x,\omega) = p_o \frac{\cos\left(k(l-x)\right)}{\cos\left(kl\right)} \tag{3}$$

$$u(x,\omega) = \frac{p_o}{\rho_o c} \frac{i\sin\left(k(l-x)\right)}{\cos\left(kl\right)} \tag{4}$$

If the pu-probe is placed at a position $x$ in the tube, the ratio between the pressure microphone of the pu-probe and the reference microphone is given by ($p_{probe} = p(x)$):

$$\frac{p_{probe}(\omega)}{p_{ref}(\omega)} = \cos\left(k(l-x)\right) \tag{5}$$

The ratio between the particle velocity at the probe and the pressure at the reference microphone equals:

$$\frac{u_{probe}(\omega)}{p_{ref}(\omega)} = \frac{i}{\rho_o c}\sin\left(k(l-x)\right) \tag{6}$$

To calibrate the phase difference between the Microflown and the pressure microphone of the pu-probe, the ratio of both is measured. Theoretically, this ratio should equal:

$$\frac{u_{probe}(\omega)}{p_{probe}(\omega)} = \frac{i}{\rho_o c}\tan\left(k(l-x)\right) \rightarrow phase\{\frac{u_{probe}(\omega)}{p_{probe}(\omega)}\} = \pm 90^\circ \tag{7}$$

In figure (2) and figure (3) an example of the amplitude calibration of the microphone and the Microflown of the pu-probe are shown respectively. The pu-probe is placed at a distance $x - l = 54\,cm$ from the rigid ending of the standing wave tube. A swept sine measurement with lock-in detection is used. At each frequency, the sound pressure and particle velocity signals are integrated during the larger of $15.625\,ms$ and $50$ periods of the source frequency.

The calibration curve of the phase difference between the miniature microphone and the Microflown of the pu-probe is shown in figure (4). The sensitivity of the microphone of the pu-probe is for this probe $21.25\,\frac{mV}{Pa}$. At low frequencies, the sensitivity of the Microflown ($lfs$) is $162.13\,\frac{mV}{Pa} \cdot \rho_o c$ and the roll-off frequencies $f_e$, $f_d$ and $f_{hc}$ are $0\,Hz$, $911\,Hz$ and $\infty$ respectively. $C_1$, $C_2$, and $C_3$ are $51\,Hz$, $885\,Hz$ and $\infty$ respectively.

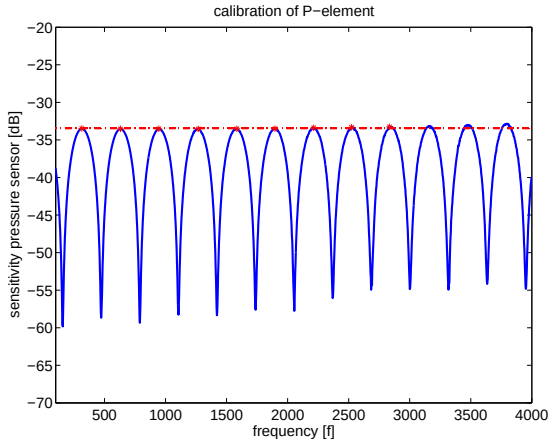


Figure 2: calibration of microphone of pu-probe

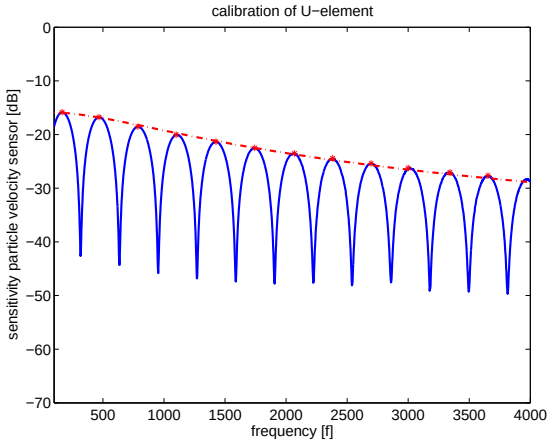


Figure 3: calibration of Microflown of pu-probe

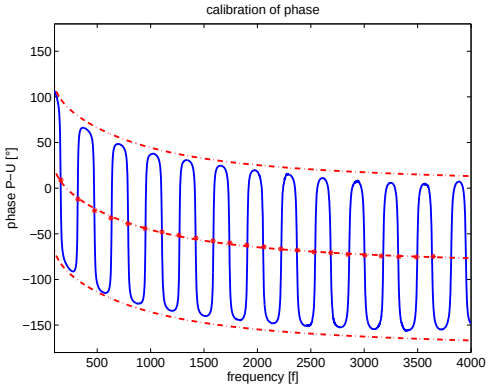


Figure 4: calibration of phase of pu-probe

### 2.1.2 Semi-anechoic room

Since no reflections are present in a semi-anechoic room if absorbing wedges are placed at the floor, a free field measurement can be performed. For a free spherical sound wave, induced by a spherical sound source at position $r = 0$, the frequency dependent impedance at a distance $r$ from the source, is given by formula (8).

$$Z(r,\omega) = \frac{p(r,\omega,t)}{u_r(r,\omega,t)} = \rho_o c \frac{ikr}{1+ikr} \tag{8}$$

The ratio will alter in formula (9) if $kr$ is much larger than unity, so if the source is placed far enough from the measurement position.

$$Z(r,\omega) = \rho_o c \tag{9}$$

The calibration setup in the semi-anechoic room is shown in figure (5).

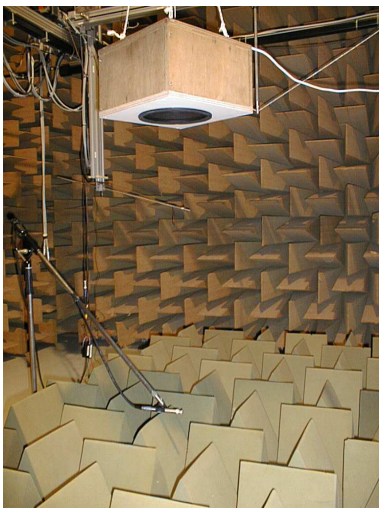

Figure 5: calibration of pu-probe in semi-anechoic room

In figures (6) and (7), the calibration values of the impedance amplitude (divided by the characteristic impedance in air, $\rho_o c$) and phase are given for different distances probe-source. The measurements were corrected for the near field effect (the calibration value is dependent of the distance probe-source (see formula (8)). A 'dip' in the frequency response of the probe around $4200\ Hz$ is clearly noticeable. This dip can be explained by the electrical tuning of the pu-probe.

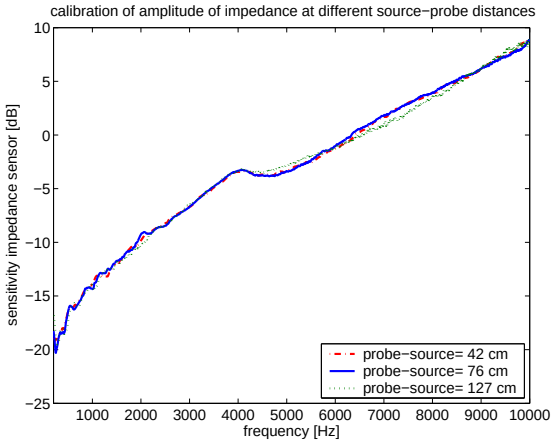


Figure 6: calibration of amplitude of pu-probe

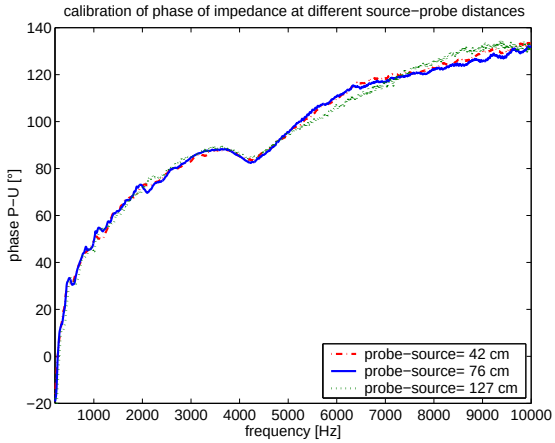


Figure 7: calibration of phase of pu-probe

In figure (8) and figure (9), the calibration values of the impedance amplitude (divided by $\rho_o c$) and phase are given for different angles of sound incidence at the probe. The vertical distance probe-source was held constant and the probe was moved horizontally in a plane parallel to the top of the absorbing wedges. In figure (8), an approximation of the calibration values for the incidence angles $45^o$ and $60^o$ is made based on the calibration values found at normal incidence by dividing these values by $\cos\theta$ with $\theta$ the incidence angle. As expected, the signal to noise ratio falls drastically at higher incidence angles and at higher frequencies (frequencies higher than $5000\,Hz$) the phase response shifts for larger incidence angles. A better signal to noise ratio can be obtained if the source is rotated and directed to the probe.

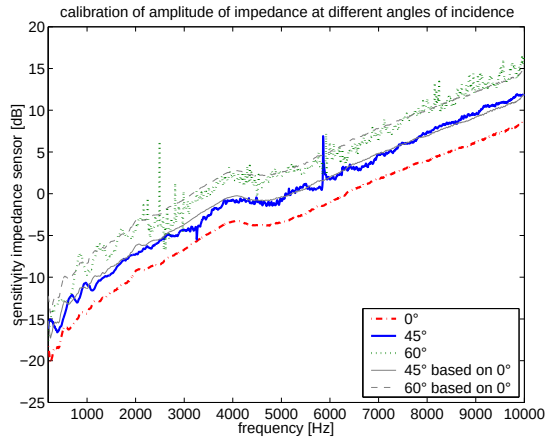


Figure 8: calibration of amplitude of pu-probe

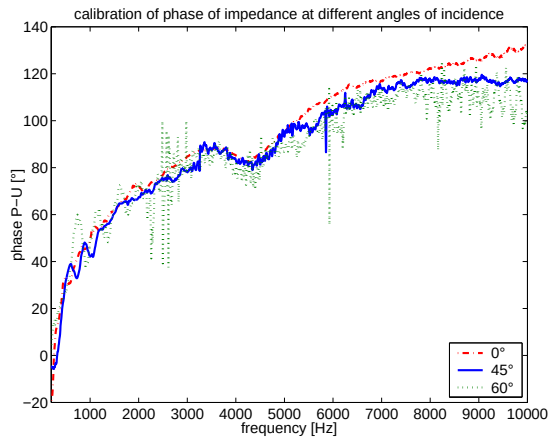


Figure 9: calibration of phase of pu-probe

# 3 Theoretical background

## 3.1 Kundt's tube

Since the acoustic field in a Kundt tube is very well known, experiments were started in this tube to examine the usefulness of the new measurement technique. A sketch of the measurement setup is given in figure (10).

In this kind of tube, a one-dimensional acoustic field is generated with a speaker placed at one end of the tube. A first incoming plane wave ($p_{in}(x,t,\omega) = p_o e^{i(\omega t + kx)}$) travels from the source to the absorbing material placed at the other end of the tube. A second wave ($p_{out}(x,t,\omega) = R(\omega) p_o e^{i(\omega t - kx)}$) travels in the opposite direction from the sample to the source. This second wave is the resulting wave after phase

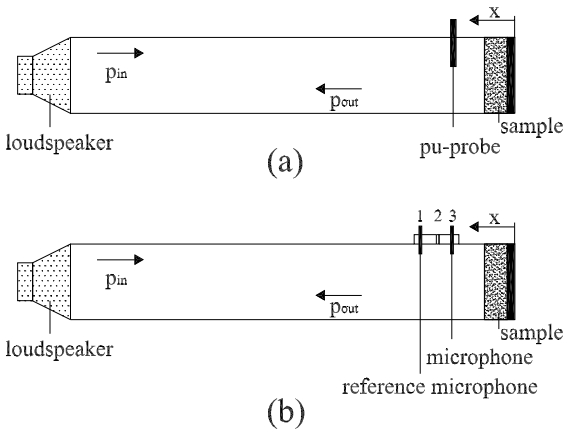


Figure 10: Kundt tube, measurement setup

rotation and attenuation of the incoming wave at the sample surface. The reflection coefficient is frequency dependent. In the tube, a standing wave is established as a result of the incoming and outgoing wave. So, the resulting pressure field in the tube can be described by:

$$p_{tot}(x,t,\omega) = p_{in}(x,t,\omega) + p_{out}(x,t,\omega) = p_o(e^{i(\omega t+kx)} + R(\omega)e^{i(\omega t-kx)}) \tag{10}$$

From the equation of momentum conservation, the particle velocity in the tube can be derived:

$$u_{tot}(x,t,\omega) = \frac{1}{\rho_o}\int \frac{\partial p_{tot}(x,t,\omega)}{\partial x}dt = \frac{p_o}{\rho_o c}(e^{i(\omega t+kx)} - R(\omega)e^{i(\omega t-kx)}) \tag{11}$$

The impedance at a position $x$ in the tube is defined by formula (12).

$$Z(x,\omega) = \frac{p_{tot}(x,\omega)}{u_{tot}(x,\omega)} = \rho_o c\frac{e^{ikx} + R(\omega)e^{-ikx}}{e^{ikx} - R(\omega)e^{-ikx}} \tag{12}$$

So, if sound pressure and sound particle velocity at a distance $x$ from the sample surface can be measured, the reflection coefficient and surface impedance of that sample can immediately be deduced:

$$R(\omega) = e^{2ikx}\frac{Z(x,\omega) - \rho_o c}{Z(x,\omega) + \rho_o c} \tag{13}$$

$$Z(0,\omega) = \rho_o c\frac{1 + R(\omega)}{1 - R(\omega)} \tag{14}$$

The acoustic absorption coefficient of the sample can be calculated by:

$$\alpha(\omega) = 1 - |R(\omega)|^2 \tag{15}$$

## 3.2 Semi-anechoic room

After measuring the absorption coefficient at normal incidence in a Kundt tube, measurements in a semi-anechoic room are performed. In this room, there can also be measured at oblique incidence. If a point source is considered, intensity will reduce proportionally with the square of the distance. Pressure amplitude reduces proportionally with the distance.

Figure (11) shows the setup for the measurement in the semi-anechoic room. Let $\theta$ be the specular angle of incidence, given by $\theta = \arctan\frac{r}{h+d}$.

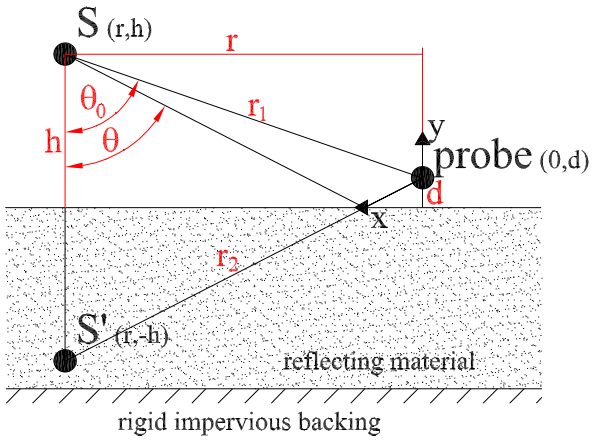


Figure 11: Free field setup, oblique incidence

The incident wave which is travelling from the source to the probe is, at the position of the probe, given by $p_{in}(0,d,t,\omega) = \frac{p_o}{r_1}e^{i(\omega t+kr_1)}$ with $r_1$ the distance between the source (S) and the probe. In this formula, $d$ is the normal distance between the probe and the sample. To include the reflection of the sample, a mirror source (S') is placed behind the sample at the same distance as the physical source is placed from the sample (see figure (11)). This assumption is only valid if the value $kr_1$ is sufficiently large [6]. The wave which is travelling from that mirror source in the direction of the probe is given by $p_{out}(0,d,t,\omega) = R(\omega,\theta)\frac{p_o}{r_2}e^{i(\omega t+kr_2)}$.

So, the total pressure at the position $(0,d)$ is given by formula (16).

$$\begin{aligned} p_{tot}(0,d,t,\omega) &= p_{in}(0,d,t,\omega) + p_{out}(0,d,t,\omega) \\ &= p_o\left(\frac{e^{i(\omega t+kr_1)}}{r_1} + R(\omega,\theta)\frac{e^{i(\omega t+kr_2)}}{r_2}\right) \\ &= p_o\left(\frac{e^{ikr_1}}{r_1} + R(\omega,\theta)\frac{e^{ikr_2}}{r_2}\right)e^{i\omega t} \end{aligned} \tag{16}$$

Formula (17) for the particle velocity, which is normal to the impedance plane, can now be deduced.

$$\begin{aligned} u_{n,tot}(0,d,t,\omega) &= u_{n,in}(0,d,t,\omega) - u_{n,out}(0,d,t,\omega) \\ &= \frac{p_o}{\rho_o c}\left[\left(\frac{1-ikr_1}{-ikr_1}\right)\frac{e^{ikr_1}}{r_1}\cos\theta_o - R(\omega,\theta)\left(\frac{1-ikr_2}{-ikr_2}\right)\frac{e^{ikr_2}}{r_2}\cos\theta\right]e^{i\omega t} \end{aligned} \tag{17}$$

Formula (18) for the impedance at the position of the probe is obtained.

$$\begin{aligned} Z(0,d,\omega) &= \frac{p_{tot}(0,d,\omega)}{u_{tot}(0,d,\omega)} \\ &= \rho_o c\,\frac{\frac{e^{ikr_1}}{r_1} + R(\omega,\theta)\frac{e^{ikr_2}}{r_2}}{\left(\frac{1-ikr_1}{-ikr_1}\right)\frac{e^{ikr_1}}{r_1}\cos\theta_o - R(\omega,\theta)\left(\frac{1-ikr_2}{-ikr_2}\right)\frac{e^{ikr_2}}{r_2}\cos\theta} \end{aligned} \tag{18}$$

From this last equation, a formula for the reflection coefficient of the absorbing surface can be deduced:

$$R(\omega,\theta) = e^{ik(r_1-r_2)}\frac{r_2}{r_1}\frac{Z(0,d,\omega)\left(\frac{1-ikr_1}{-ikr_1}\right)\cos\theta - \rho_o c}{Z(0,d,\omega)\left(\frac{1-ikr_2}{-ikr_2}\right)\cos\theta_o + \rho_o c} \tag{19}$$

If the pu-probe is placed very close to the surface ($d$ is very small), $\theta \simeq \theta_o$ and $r_1 \simeq r_2$. So, equation (19) becomes:

$$R(\omega,\theta) \simeq \frac{Z(0,d,\omega)(\frac{1-ikr_1}{-ikr_1})\cos\theta - \rho_o c}{Z(0,d,\omega)(\frac{1-ikr_1}{-ikr_1})\cos\theta + \rho_o c} \tag{20}$$

Since the mirror-source-model is only valid if $kr_1$ is sufficiently large, formula (20) becomes formula (21), which equals the formula for plane sources.

$$R(\omega,\theta) \simeq \frac{Z(0,d,\omega)\cos\theta - \rho_o c}{Z(0,d,\omega)\cos\theta + \rho_o c} \tag{21}$$

# 4 Experimental results

## 4.1 Kundt's tube

The properties of the absorbing sample are given in table (1). A prediction of the absorption coefficient can be made based on the model of Biot-Johnson-Allard [7, 8] from the parameters of table (1).

| Thickness $l\,[m]$ | Density $\rho\,[\frac{kg}{m^3}]$ | Tortuosity $\alpha_\infty$ | Porosity $\phi$ | Flow resistivity $\sigma\,[\frac{Ns}{m^4}]$ | Viscous length $\Lambda\,[\mu m]$ | Thermal length $\Lambda'\,[\mu m]$ |
|---|---|---|---|---|---|---|
| 0.03 | 14 | 1.09 | 0.98 | 10500 | 100 | 150 |

Table 1: Properties of studied porous material

The results of a measurement of the porous material in a Kundt tube (see figure (10(a))) with diameter $3.9\,cm$ and the pu-probe placed at a distance of $2.5\,cm$ from the sample surface, are given in figure (12). The considered frequencies are low enough to assure plane propagating waves in the tube (cut-off frequency $f_c \simeq 5000\,Hz$). A good correspondence between the simulated curve and the pu-technique is reached. Since the calibration in Kundt's tube is valid up to $\pm 3200\,Hz$, only the results up to this frequency are shown. A second measurement is also shown in this figure. This measurement is done by measuring the sound pressure at two positions in the tube, called the pp-technique (see figure 10(b)). The dip in this measurement curve is due to the fact that one of the microphones lies at a pressure minimum at that frequency.

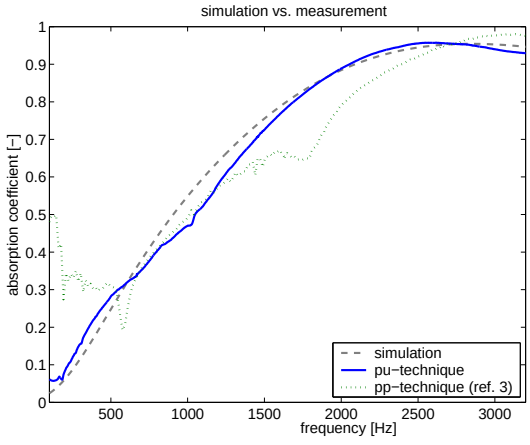


Figure 12: Kundt measurement, simulation vs. measurement

## 4.2 Semi-anechoic room

Measurements in the semi-anechoic room were executed on the same test material (properties, see table (1)). An absorbing sample surface of $2.2\,m^2$ was used and the measurement time to obtain the absorption coefficient for a certain incidence angle was less than 10 minutes for the chosen frequency range.

First, a measurement of the impedance at normal sound incidence was performed. The source was placed at different heights above the pu-probe, which was placed directly on the absorbing surface. So, the distance between the sample and the Microflown and microphone was $\pm\,6\,mm$. The probe-source distances were taken equal to the values chosen for the calibration in the free field conditions. The absorption coefficient of the material can be calculated with formula (20) and formula (21) if $kr \gg 1$. The results of this measurements, together with a simulation based on the model of Biot-Johnson-Allard are given in figure (13). Next to the measurements with the pu-probe and the simulation based on the theoretical model, a last curve is shown. These measurements are deduced from a Tamura measurement on a sample surface of $\pm\,10\,m^2$. A measurement time of $4$ hours is needed to deduce the absorption coefficient for all incidence angles in the chosen frequency range ($200\,Hz - 8\,kHz$). There's a good correspondence between the results of both measurement techniques.

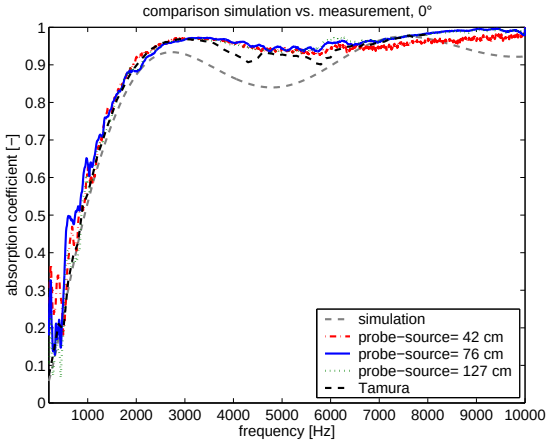


Figure 13: Measurement in semi-anechoic room, incidence $0^o$

Next to the measurement at normal incidence, measurements at oblique incidence were performed.

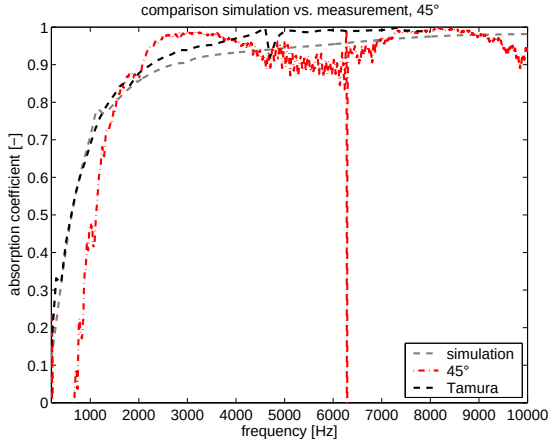


Figure 14: Measurement in semi-anechoic room, incidence $45^o$

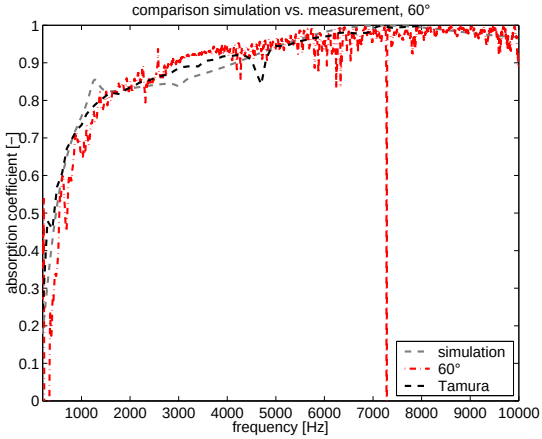


Figure 15: Measurement in semi-anechoic room, incidence $60^o$

The vertical distance probe-source was kept $76\,cm$ and the probe was moved over the absorbing surface. The results for an incidence angle of $45^o$ and $60^o$ are respectively shown in figure (14) and in figure (15). As expected, these measurements are, at higher frequencies, influenced by noise. The results of the Tamura measurement are also shown in both figures.

# 5 Conclusion

In this paper, results of measurements with a pu-probe, consisting of a Microflown and a miniature microphone are presented. In first order, a few calibration mechanisms in a Kundt tube and in a semi-anechoic room are presented. In both methods, measurements are compared to the well known sound field to obtain the calibration values of the pu-probe.
Afterwards, the absorption coefficient of a sound absorbing sample is measured in a Kundt tube and in a semi-anechoic room. It's shown that the pu-probe can be a very attractive measurement technique. The sensitivity of the Microflown to the direction of the waves is very useful and makes measurements very simple. The advantages of the measurement with a pu-probe are the smaller sample size, the smaller measurement time and the simpler mathematics compared to the Tamura technique. Another advantage is the fact that out of the measurement at a certain position the absorption coefficient for that incidence angle can be deduced. The Tamura technique needs a measurement at all angles before one can deduce the absorption coefficient for a certain incidence angle.

# 6 Further research

A better signal to noise ratio can be obtained by directing the source to the pu-probe and by integrating the signals over a longer time period. So, a rotating and smaller source can be used in further research. Also a smaller protective cap can probably deliver more accurate measuring results. In figure (16) a possible new design of the pu-probe is shown.

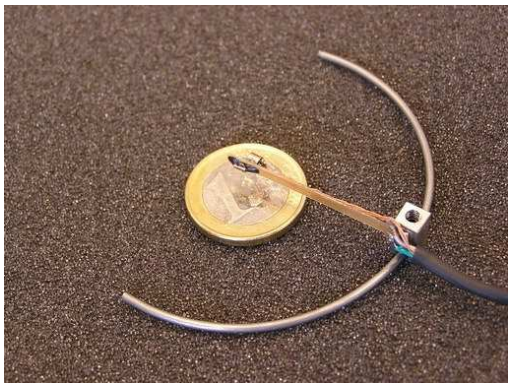

Figure 16: New design of the pu-probe

Before one can start using the pu-technique for in-situ measurements, the influence of the distance sample-probe on the necessary size of the sample has to be investigated.

## References


[1] Tamura, M., *Spatial Fourier-Transform Method of Measuring Reflection Coefficients at Oblique-Incidence .1. Theory and Numerical Examples*, Journal of the Acoustical Society of America, 88(5), (1990), pp.2259-2264.

[2] Nocke, C., *In-situ acoustic impedance measurement using a free-field transfer function method*, Applied Acoustics, 59(3), (2000), pp.253-264.

[3] Chu, W. T., *Transfer-Function Technique for Impedance and Absorption-Measurements in An Impedance Tube Using A Single Microphone*, Journal of the Acoustical Society of America, 80(2), (1986), pp.555-560.

[4] Bree, H.-E. de, Leussink, P.J., Korthorst, M.T., Jansen, H.V., Lammerink, T., and Elwenspoek, M., *The Microflown: a novel device measuring acoustical flows*, Sensors and Actuators A-Physical, 54, (1996), pp.552-557.

[5] Bree, H.-E. de, Lammerink, T., Elwenspoek, M., Fluitman, J., Patent PCT/NL95/00220, *Use of a fluid flow measuring device as a microphone and system comprising such a microphone*, 1995.

[6] Rudnick, I., *The propagation of an acoustic wave along a boundary*, Journal of the Acoustical Society of America, 19, (1947), pp.348-356.

[7] Allard, J. F., *Propagation of sound in porous media*, (1993).

[8] Johnson, D. L., Koplik, J., and Dashen, R., *Theory of Dynamic Permeability and Tortuosity in Fluid-Saturated Porous-Media*, Journal of Fluid Mechanics, 176, (1987), pp.379-402.